Published online 3 October 2020

Nucleic Acids Research, 2020, Vol. 48, No. 19 ***10739–10752***
doi: 10.1093/nar/gkaa776

A genetic screen for suppressors of hyper-repression of the fission yeast *PHO* regulon by Pol2 CTD mutation T4A implicates inositol 1-pyrophosphates as agonists of precocious lncRNA transcription termination

Angad Garg [1], Stewart Shuman [1,*] and Beate Schwer[2,*]

[1]Molecular Biology Program, Sloan-Kettering Institute, New York, NY 10065, USA and [2]Department of Microbiology and Immunology, Weill Cornell Medical College, New York, NY 10065, USA

Received August 04, 2020; Revised September 03, 2020; Editorial Decision September 05, 2020; Accepted September 29, 2020

ABSTRACT

Fission yeast phosphate homeostasis genes are repressed in phosphate-rich medium by transcription of upstream lncRNAs that interferes with activation of the flanking mRNA promoters. lncRNA control of *PHO* gene expression is influenced by the Thr4 phospho-site in the RNA polymerase II CTD and the 3′ processing/termination factors CPF and Rhn1, mutations of which result in hyper-repression of the *PHO* regulon. Here, we performed a forward genetic screen for mutations that de-repress Pho1 acid phosphatase expression in *CTD-T4A* cells. Sequencing of 18 independent *STF* (Suppressor of Threonine Four) isolates revealed, in every case, a mutation in the C-terminal pyrophosphatase domain of Asp1, a bifunctional inositol pyrophosphate (IPP) kinase/pyrophosphatase that interconverts 5-IP7 and 1,5-IP8. Focused characterization of two *STF* strains identified 51 coding genes coordinately upregulated *vis-à-vis* the parental *T4A* strain, including all three *PHO* regulon genes (*pho1*, *pho84*, *tgp1*). Whereas these *STF* alleles—*asp1-386(Stop)* and *asp1-493(Stop)*—were lethal in a wild-type CTD background, they were viable in combination with mutations in CPF and Rhn1, in which context Pho1 was also de-repressed. Our findings implicate Asp1 pyrophosphatase in constraining 1,5-IP8 or 1-IP7 synthesis by Asp1 kinase, without which 1-IPPs can accumulate to toxic levels that elicit precocious termination by CPF/Rhn1.

INTRODUCTION

The carboxyl-terminal domain (CTD) of the Rpb1 subunit of RNA polymerase II (Pol2), comprising tandemly repeated heptapeptides of consensus sequence $Y^1S^2P^3T^4S^5P^6S^7$, serves as a scaffold to recruit proteins that regulate transcription initiation, elongation and termination, adjust chromatin structure, and catalyze or regulate mRNA capping, splicing and polyadenylation. The primary structure of the CTD, which is dynamically sculpted by serine, threonine, and tyrosine phosphorylation and by *cis–trans* proline isomerization, conveys information about the status of the transcription machinery—a CTD code—that is 'read' by CTD-interacting proteins and RNA processing assemblies (1–5).

Our aims have been to decipher the informational rules for the CTD code by genetically manipulating the composition and structure of the fission yeast Pol2 CTD; to understand how CTD coding 'letters' are assembled into 'words' (i.e. a vocabulary); and to elucidate how CTD coding cues govern specific cellular gene expression programs (6–10). The findings that fission yeast is viable when the CTD Tyr1, Ser2, Thr4 or Ser7 residues are uniformly replaced by a non-phosphorylatable side chain accords with transcriptome analyses showing that only a small fraction of fission yeast mRNAs is dysregulated by CTD phospho-site mutations. We hypothesized that the effects of mutating these phospho-sites are genetically buffered by other cellular factors that are functionally redundant to the phospho-mark or the side-chain hydroxyl. By identifying such functional redundancies (manifest as synthetic lethality), and gauging their specificity for a particular phospho-site mutation, we showed that the effects of mutating the inessential Tyr1, Ser2, and Thr4 CTD phospho-sites on fission yeast cell growth are buffered by subunits of the fission yeast cleavage and polyadenylation factor (CPF) complex (10).

*To whom correspondence should be addressed. Tel: +1 212 639 7145; Email: s-shuman@ski.mskcc.org
Correspondence may also be addressed to Beate Schwer. Tel: +1 212 746 6518; Email: bschwer@med.cornell.edu

Key insights emerged from studies of fission yeast phosphate homeostasis, a transcriptional response to phosphate availability that is governed by the CTD code and the 3′ processing/termination machinery (8–12). The *Schizosaccharomyces pombe* phosphate (*PHO*) regulon comprises three genes that specify, respectively, a cell surface acid phosphatase Pho1, an inorganic phosphate transporter Pho84, and a glycerophosphate transporter Tgp1 (13). Expression of the *PHO* genes *pho1*, *pho84*, and *tgp1* is actively repressed during growth in phosphate-rich medium by the transcription in *cis* of a long noncoding (lnc) RNA from the respective 5′ flanking genes *prt*, *prt2*, and *nc-tgp1* (11–12,14–17). A *CTD-S7A* allele that prevents installation of the Ser7-PO_4 mark in all heptads de-represses the *PHO* genes in phosphate-replete cells (8–10). By contrast, a *CTD-T4A* allele that precludes inscription of the Thr4-PO_4 mark hyper-represses *PHO* genes under phosphate-rich conditions (8–10). Our model for the repressive arm of phosphate homeostasis is that: (i) transcription of the upstream lncRNA interferes with expression of the downstream mRNA genes by displacing the activating transcription factor Pho7 from its binding site(s) in the mRNA promoters that overlap the lncRNA transcription units (13,18–20); (ii) loss of the Ser7-PO_4 mark leads to precocious termination of lncRNA transcription prior to the mRNA promoter; and (iii) loss of the Thr4-PO_4 mark reduces termination and hence increased transcription across the mRNA promoter (10). This model is supported by RNA analyses, transcriptomics and epistatic effects of CTD mutations with mutations of CPF subunits and transcription termination factor Rhn1 (10).

A model for the transcriptional arm of the fission yeast phosphate starvation response is that phosphate deprivation triggers a signaling pathway that ultimately results in shut-off of transcription of the *prt*, *prt2*, and *nc-tgp1* lncRNAs that—under phosphate replete conditions—interfere in *cis* with expression of the downstream *pho1*, *pho84*, and *tgp1* phosphate acquisition genes (11). Yet, the mechanism of phosphate sensing in fission yeast is obscure and it is not known how a starvation signal is transmitted to impact lncRNA transcription initiation by Pol2. Our work has defined a distinctive bipartite promoter—consisting of a HomolD box and a TATA box—that is essential for transcription of the three *PHO*-regulatory lncRNAs (11–12,14). The transcription factors that recognize the lncRNA promoters (particularly the HomolD box) and drive lncRNA synthesis are uncharted. The HomolD box [5′-CAGTCAC(A/G)] was identified initially as a Pol2 promoter signal in fission yeast genes encoding ribosomal proteins (21–23). Mutations in the lncRNA or in protein factors that diminish lncRNA 3′ processing/termination can delay, but do not eliminate, the upregulation of *PHO* gene transcription in response to phosphate starvation (9,11–12).

A notable outcome of our epistasis analyses, wherein we made pairwise combinations of the hyper-repressive *CTD-T4A* allele with various mutations that de-repress the *PHO* regulon in phosphate-replete cells, was that *T4A* repression generally 'won out' over de-repression (9,10). This signifies that the de-repressive mutations, which are posited to elicit precocious lncRNA termination, depend on Thr4-PO_4 (or the Thr4 hydroxyl) to achieve their effect. Our aim in the present study was to query how the *T4A* mutant affects 3′ processing/termination, by performing a genetic screen in *CTD-T4A* cells for extragenic suppressors of the *pho1* hyper-repressive phenotype. We felt this was an auspicious scenario for suppressor genetics, because it is virtually impossible to obtain a revertant of the *rpb1-CTD-T4A* allele that has 27 different missense codon mutations that change Thr to Ala, and because the known mutations that de-repress *pho1* in a wild-type CTD background ought not to score as such in *T4A* cells. We envisioned two potential classes of *T4A* suppressor mutations: (i) those that reduce or shut off transcription of the *prt* lncRNA and thereby relieve *prt* interference with the *pho1* promoter; and (ii) those that enhance the 3′ processing/termination efficiency of the T4A mutant Pol2 transcription complex engaged in *prt* lncRNA synthesis. With respect to the latter category, we can imagine several ways in which *T4A* might be suppressed. For example, by mutations in Pol2 itself (e.g. mutations that affect its elongation properties or CTD-independent interactions with elongation, processing and termination factors); by mutations in Pol2 elongation factors (that affect the temporal window to elicit termination of lncRNA synthesis); by hypomorphic mutations in essential 3′ processing/termination factors for which we presently have no genetic handles to establish their connections to the CTD code; by mutations that influence rNTP pools and thereby affect Pol2 elongation indirectly; or by mutations that affect the levels of signaling molecules that regulate 3′ processing/termination.

We describe here the isolation and characterization of a collection of *STF* (Suppressor of Threonine Four) mutants. Sequencing of 18 independent *STF* isolates revealed, in every case, missense or nonsense mutations in the C-terminal pyrophosphatase domain of Asp1—a bifunctional inositol pyrophosphate (IPP) kinase/pyrophosphatase enzyme (24–28)—as responsible for the *STF* phenotype. Epistasis analysis *vis-à-vis* CPF and Rhn1 indicates that *STF* mutations promote 3′ processing/termination. Transcriptional profiling uncovered an ensemble of 51 coding genes that were coordinately up-regulated in two different *STF* nonsense mutant strains; this set includes all three genes of the *PHO* regulon. Thus, our forward genetic screen fortifies the recent proposal (29) that fission yeast phosphate homeostasis is subject to metabolite control by inositol pyrophosphates, exerted via the 3′ processing/termination machinery and the Pol2 CTD.

MATERIALS AND METHODS

Mutagenesis of *rpb1-CTD-T4A* cells and screening for increased *pho1* expression

Ethyl methanesulfonate (EMS) mutagenesis was carried out as described (30). In brief, *rpb1-CTD-T4A* cells were grown in minimal medium (PMG) at 30°C to an A_{600} of 0.25. Cells were harvested by centrifugation and resuspended at ∼1 × 10^8 cells/ml in PMG medium. To one aliquot (2 ml), we added EMS (Sigma) to a final concentration of 2%, while a second aliquot was left untreated (to determine survival rate). The suspensions were placed on a nutator and incubated for 3.5 h at room temperature. Cells were washed thrice with NaCl (150 mM), diluted, and plated to YES

agar. After 5 days of incubation at 30°C, plates were overlaid with 1% agarose containing 0.015% α-naphthyl phosphate, 0.15% Fast Blue B Salt stain, and 0.1 M sodium acetate (pH 4.2) to assay acid phosphatase activity. Colonies that turned red were extracted from near confluent lawns of mutagenized cells and colony-purified by streaking or re-plating at low cell densities. Independently isolated candidate suppressor strains were back-crossed to *rpb1-CTD-T4A* cells of the opposite mating type, subjected to random spore analysis, and identified as red colonies using the overlay assay. After back-crossing individual suppressor strains for a second time, we measured acid phosphatase activity of cells grown in liquid culture (YES medium) at 30°C, as follows. Exponentially growing cultures were harvested, washed, and resuspended in water. Reaction mixtures (200 μl) containing 10 mM *p*-nitrophenylphosphate, 100 mM sodium acetate (pH 4.2), and serial dilution of cells (ranging from 0.01 to 0.1 A_{600} units) were incubated at 30°C for 5 min. To stop the reaction, 1 ml of 1 M sodium carbonate was added, the cells were removed by centrifugation, and the absorbance of the supernatant at 410 nm was measured. Acid phosphatase activity is expressed as the ratio of A_{410} (*p*-nitrophenol production) to A_{600} (cells). The data are averages (±SEM) of measurements from at least three independent cultures.

Spot tests of fission yeast growth

Cultures of *S. pombe* strains were grown in liquid YES (yeast extract with supplement) medium until A_{600} reached 0.5–0.8. The cultures were adjusted to an A_{600} of 0.1 and aliquots (3 μl) of serial 5-fold dilutions were spotted to YES agar. The plates were photographed after incubation for 2 days at 34°C, 2.5 days at 30°C and 37°C, 4 days at 25°C, and 6 days at 20°C.

Whole-genome sequencing

After PicoGreen quantification and quality control by Agilent BioAnalyzer, 500 ng aliquots of genomic DNA were sheared using a LE220-plus Focused-ultrasonicator (Covaris catalog # 500569) and sequencing libraries were prepared using the KAPA Hyper Prep Kit (Kapa Biosystems KK8504) with modifications. DNA libraries were subjected to size selection by mixture with 0.5 volume of aMPure XP beads (Beckman Coulter catalog # A63882) after post-ligation cleanup. Libraries were not amplified by polymerase chain reaction (PCR) and were pooled equivolume for sequencing. Samples were run on a NovaSeq 6000 in a 150/150 bp paired end run using the NovaSeq 6000 SBS v1 Kit and an S1 flow cell (Illumina). The average number of read pairs per sample was 10 million.

Mapping *STF* mutations

The FASTA file for the *S. pombe* genome was accessed from Pombase and modified by replacing the wild-type *rpb1* locus with the *rpb1-CTD-T4A* allele sequence. To preserve chromosomal coordinates of all other genes, the *natMX* antibiotic-resistance gene and *TPI1* terminator sequences placed 3′ of the *rpb1-CTD-T4A* ORF during strain construction were annotated separately in the genome FASTA file. The genome index was built from this modified FASTA file using Bowtie2 (31). The whole-genome sequencing data from the parental and *STF* mutant *rpb1-CTD-T4A* strains were aligned to the genome using Bowtie2 (31). The resulting SAM files were converted to BAM files using Samtools (32). Variants were identified by BCFtools (33) using the criteria of adjusted mapping quality = 40, minimum base quality = 20, and disabled probabilistic realignment for the computation of base alignment quality for considering variations or insertion-deletion events. The multi-allelic caller protocol was used for variant calling in BCFtools. Variants were annotated using SnpEff, with its in-built genome version for *S. pombe* (34). Variants were further filtered by removing all variations with an average mapping quality ≤25 (Phred scale). All variants present in the parental strain were excluded as non-causal mutations.

Transcriptome profiling by RNA-seq

RNA was isolated from *S. pombe STF-6* and *STF-9* cells and from parental *CTD-T4A* cells that were grown in liquid YES medium at 30°C to an A_{600} of 0.5–0.6. Cells were harvested by centrifugation and total RNA was extracted via the hot phenol method. The integrity of total RNA was gauged with an Agilent Technologies 2100 Bioanalyzer. The Illumina TruSeq stranded mRNA sample preparation kit was used to purify poly(A)$^+$ RNA from 500 ng of total RNA and to carry out the subsequent steps of poly(A)$^+$ RNA fragmentation, strand-specific cDNA synthesis, indexing, and amplification. Indexed libraries were normalized and pooled for paired-end sequencing performed by using an Illumina NovaSeq 6000-S1 flow cell. FASTQ files bearing paired-end reads of length 51 bases were mapped to the *S. pombe* genome (Pombase) using HISAT2-2.1.0 with default parameters (35). The resulting SAM files were converted to BAM files using Samtools (32). Count files for individual replicates were generated with HTSeq-0.10.0 (36) using exon annotations from Pombase (GFF annotations, genome-version ASM294v2; source 'ensembl'). RPKM analysis and pairwise correlations (Supplementary Figures S1 and S2) were performed as described previously (8). Differential gene expression and fold change analysis was performed in DESeq2 (37). Cut-off for further evaluation was set for genes that had an adjusted p-value (Benjamini–Hochberg corrected) of ≤0.05 and were up or down by at least 2-fold in *STF-6* or *STF-9* in comparison to *CTD-T4A*. Genes were further filtered on the following criteria: (i) ≥2-fold up and the average normalized read count for the mutant strain was ≥100; and (ii) ≥2-fold down and the average normalized read count for the parent strain was ≥100.

RESULTS

The *STF* screen

rpb1-CTD-T4A cells were mutagenized by treatment with 2% EMS for 3.5 h at 22°C to achieve a survival rate of ∼40%. The cells were washed, plated on phosphate-replete YES agar medium, and incubated for 5 days at 30°C to allow formation of single colonies from individual mutagenized cells. To gauge acid phosphatase activity, the

plates were overlaid with 1% agarose containing 0.015% α-naphthyl phosphate (a Pho1 substrate), 0.15% Fast Blue B Salt stain, and 0.1 M sodium acetate (pH 4.2). The cell surface Pho1 acid phosphatase causes formation of a red pigment and relative red color intensity of the colonies provides a semi-quantitative assay of Pho1 activity (8,38). *T4A* cells appear pale after this procedure. From an initial pool of about 390 000 EMS survivors, we picked 50 independent red colonies that we deemed candidate *STF* mutants. These were re-streaked for single colonies, then grown out in YES liquid medium, re-plated, and re-tested for red color. We then selected 36 of the most intensely red straining strains, back-crossed them to a *T4A* strain of the opposite mating type, and tested populations of post-sporulation haploid progeny for Pho1 acid phosphatase activity via the overlay assay. If the *STF* phenotype results from a mutation in a single gene, then we expect ∼50% of the haploid progeny from the back-cross to stain red and ∼50% to be pale. An example of such segregation is shown in Figure 1A. Twenty-four of the back-crossed putative single-gene *STF* mutants were back-crossed for a second time to the original parental *T4A* strain and 1:1 segregation of red/pale colony color was affirmed. Twelve independent twice back-crossed *STF* strains and the parental *T4A* strain were assayed quantitatively for Pho1 activity after growth at 30°C in phosphate-replete liquid medium. The *STF* strains expressed 23- to 49-fold higher Pho1 activity than the *T4A* parent (Figure 1B). All twelve of these *STF* strains grew as well as the *T4A* parent on YES agar at 30°C (Figure 1C).

Identification of *STF* mutations by whole genome sequencing

Paired-end Illumina sequencing of unamplified genomic DNA (average read length 150 bases) from the parental *T4A* strain and the twelve *STF* strains was performed by the MSKCC genomics core facility to achieve at least 100-fold coverage of each fission yeast genome. The striking finding was that 12/12 *STF* strains had acquired missense or nonsense mutations in the *asp1*$^+$ gene that encodes a bifunctional kinase/pyrophosphatase enzyme involved in inositol pyrophosphate (IPP) metabolism (24–28) (Supplementary Figure S3). A list of missense, nonsense or frameshift mutations within other coding genes that were detected in the 12 *STF* strains *vis-à-vis* the parental *T4A* strain is shown in Supplementary Figure S3. In cases where the same mutation was found in multiple different *STF* strain genomes, it is most likely that they were acquired as polymorphisms from the *T4A* strain of opposite mating type that was employed during the two rounds of back-crossing prior to whole-genome sequencing. This is certainly the case for the *ade6-(P489L)* coding mutation found in 7/12 of the *STF* strains (Supplementary Figure S3), i.e. this *ade6* allele (known as *ade6-M210*) is an auxotrophic marker used to select diploids after mating.

Three pairs of *STF* strains had an identical nucleobase mutation in the *asp1*$^+$ open reading frame: *STF-6* and *STF-10* (G1158A); *STF-5* and *STF-8* (G1928A); *STF-3* and *STF-11* (G2588A). Although *STF-6* and *STF-10* have the same *asp1*$^+$ mutation, *STF-10* has two additional changes (in the *dnt1*$^+$ and *yta12*$^+$ genes) that are not found in *STF-6* or any of the other *STF* strains (Supplementary Figure S3). Similarly, whereas *STF-5* and *STF-8* have the same *asp1*$^+$ mutation, *STF-8* has a mutation (in *mgl1*$^+$) that is not found in *STF-5* or any of the other *STF* strains (Supplementary Figure S3). And, though *STF*-3 and *STF-11* have the same *asp1*$^+$ mutation, *STF-3* has 12 additional coding mutations that are not present in *STF-11* or any of the other *STF* strains (Supplementary Figure S3). We surmise that these *STF* strains are independent isolates.

The 920-aa Asp1 protein, which was mutated in all of the *STF* strains, consists of two catalytic domains: an N-terminal IPP kinase module (aa 1–364) that converts 5-IP7 to 1,5-IP8; and a C-terminal IPP pyrophosphatase domain that converts 1,5-IP8 back to 5-IP7 (Figure 2B). Asp1 can also phosphorylate IP6 to yield 1-IP7 and dephosphorylate 1-IP7 back to IP6. Asp1 is inessential for fission yeast growth. The effect of an *asp1*Δ null allele or a kinase-defective *asp1* missense mutant is to eliminate intracellular IP8 and 1-IP7 and to increase the level of 5-IP7 (26,28). Conversely, a pyrophosphatase-defective *asp1* missense mutant increases the intracellular level of IP8, as does expression of a C-terminal truncation allele that retains the kinase domain but lacks the pyrophosphatase domain (26).

Recent studies show that failure to synthesize IP8 and 1-IP7 in Asp1 null or Asp1 kinase-defective strains results in hyper-repression of the *PHO* regulon under phosphate-replete conditions (29). Synthetic lethalities of *asp1*Δ and *asp1* kinase-defective alleles with mutations of CPF subunits Ppn1, Swd22, and Ssu72 point to an important role for IP8 (or 1-IP7) in essential 3′ processing/termination events, albeit in a manner genetically redundant to CPF (29). Pertinent to the present suppressor analysis is the observation that *asp1*Δ and the kinase-defective allele are synthetically lethal with *CTD-T4A* (B. Schwer, unpublished), i.e. the negative effect of *T4A* on 3′ processing/termination is exacerbated by the lack of IP8.

The salient finding here is that all of the *STF* mutations map to the C-terminal pyrophosphatase domain of Asp1 (Figure 2A). Asp1 pyrophosphatase is a member of the histidine acid phosphatase superfamily of phosphohydrolases that act via a covalent enzyme-(histidinyl-N)-phosphate intermediate (39). (Pho1 is a member of the same acid phosphatase superfamily.) The signature active site motif—^{396}RHADR^{400} in the Asp1 pyrophosphatase—is located close to the N-terminal margin of the domain at residue 365. His397 in this motif is the Asp1 catalytic nucleophile. To aid in interpreting the *STF* mutations, we submitted the pyrophosphatase domain amino acid sequence to the Phyre2 structure modeling server (40), which returned a 'top hit' tertiary structure model templated on the 1.7 Å crystal structure of *Yersinia kristensenii* phytase (PDB ID: 4ARV; 39). The model starts at Trp386 and ends at Asp871 and is punctuated by gaps (aa 426–491, 641–659 and 699–738) comprising segments of the Asp1 pyrophosphatase that have no counterparts in *Yersinia* phytase. A stereo view of the Asp1 Phyre2 model is shown in Figure 2C with a phosphate anion in the active site derived from a superposition of the *Yersinia* phytase structure. The model places the His397-Nε nucleophile 3.3 Å from the phosphorus center and allows for a network of phosphate contacts to conserved arginine side chains Arg396, Arg400, and Arg536 (Figure 2C). Alanine mutations of Arg396,

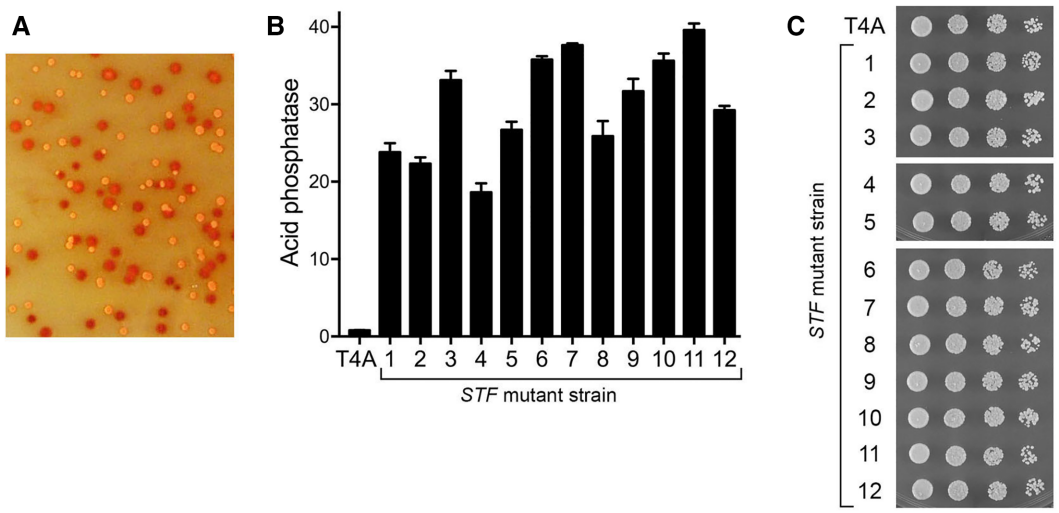

Figure 1. Isolation of fission yeast *STF* mutants. (**A**) An *STF* strain was back-crossed to a *T4A* strain of the opposite mating type and a population of post-sporulation haploid progeny grown on YES agar medium was tested for Pho1 acid phosphatase activity via the overlay assay, which revealed ∼1:1 segregation of red:pale colony color. (**B**) The indicated fission yeast strains were grown to A_{600} of 0.5–0.8 in liquid culture in YES medium at 30°C. Cells were then harvested, washed with water, and assayed for Pho1 acid phosphatase activity by conversion of *p*-nitrophenylphosphate to *p*-nitrophenol. Activity is expressed as the ratio of A_{410} (*p*-nitrophenol production) to A_{600} (input cells). (**C**) Serial 5-fold dilutions of the indicated strains were spotted on YES agar and grown for 2.5 days at 30°C.

His397, and Arg400 efface the IPP pyrophosphatase activity of the recombinant Asp1 pyrophosphatase domain (26).

Four of the *STF* alleles are nonsense mutations that leave the kinase domain intact but either eliminate the entire pyrophosphatase domain (Trp386-Stop) or truncate it at sites that would likely disrupt the tertiary structure of the domain (Trp493-Stop, Ser585-Stop, and Arg791-Stop). Thus, we assume that the *STF* nonsense mutants are catalytically pyrophosphatase-dead. The missense *STF* mutation Ala398Val is located within the ^{396}RHADR^{400} active site motif. In the Phyre2 model, the Ala398 side chain is oriented away from the active site pocket in the direction of a flanking α helix; introduction of a bulkier valine would create a steric clash and likely perturb the conformation of the active site. The missense *STF* mutation His686Tyr is located in a predicted α helix that abuts the 'back' side of the ^{396}RHADR^{400} active site motif. The His686 side chain makes van der Waals contacts with the Arg400 Cα; its replacement with a larger tyrosine side chain would create a steric clash with the main chain of the active site motif and thereby affect its conformation. Thus, we infer that *asp1-H686Y* and *asp1-A398V* strains are defective for Asp1 pyrophosphatase activity. To our inspection, the model does not provide insights to any structural defects of the Gly762Ser and Gly863Asp *STF* mutations, which are predicted to be remote from the active site. The missense *STF* mutation Cys643Tyr is located in a segment that is omitted from the Phyre2 model.

STF alleles *asp1*-(*W386-Stop*) and *asp1*-(*W493-Stop*) are lethal in a wild-type *rpb1-CTD* background

We crossed the *STF-6* and *STF-9* strains, in which the *rpb1-CTD-T4A* locus was flanked by a downstream nourseothricin-resistance marker, with a wild-type *rpb1-CTD* strain in which the *rpb1*$^{+}$ allele was flanked by a G418-resistance marker. The G418/nourseothricin-resistant diploids were sporulated and random populations of >1000 haploid progeny were selected for the resistance markers linked to the *rpb1-CTD-WT* and *rpb1-CTD-T4A* alleles. Populations of *CTD-T4A* cells were screened for Pho1 expression by agar overlay, with deep red color indicating presence of the *STF* mutation. As expected, half of the progeny were pale and half were dark red. By contrast, the yield of viable *CTD-WT* progeny was diminished by about half compared to the *CTD-T4A* progeny and all of the colonies were lightly stained red (i.e. reflecting the fact that the basal level of 'repressed' Pho1 activity in *CTD-WT* cells is several fold higher than the 'hyper-repressed' Pho1 state in *CTD-T4A* cells). With longer incubation under the agar overlay, tiny puncta of red staining were observed on the plates selective for *CTD-WT* progeny. Microscopic examination indicated that these puncta corresponded to progeny that had germinated and undergone only a few rounds of cell division. Our inference from these findings is that these two nonsense *asp1-STF* alleles are lethal in a wild-type *rpb1-CTD* background. Consistent with this interpretation, we genotyped the *asp1* locus of 12 individual *CTD-WT* isolates from the *STF-6* backcross and 12 individual *CTD-WT* isolates from the *STF-9* backcross, and found that all of them were wild-type with respect to the Asp1 pyrophosphatase domain.

To affirm the results of the random spore analysis, we dissected nine individual four-spore asci from the *STF-9* backcross and genotyped the viable haploid progeny for the *rpb1*-linked drug resistance markers and for Pho1 expression by agar overlay. Examples of the tetrad analysis are shown in Figure 3. The tetrads that yielded four viable progeny ($n = 4$) were found to be parental ditypes (PD) comprising two *CTD-T4A* dark red progeny and two *CTD-WT* light red progeny. Tetrads that yielded two viable progeny ($n = 3$) were non-parental ditypes (NPD) consist-

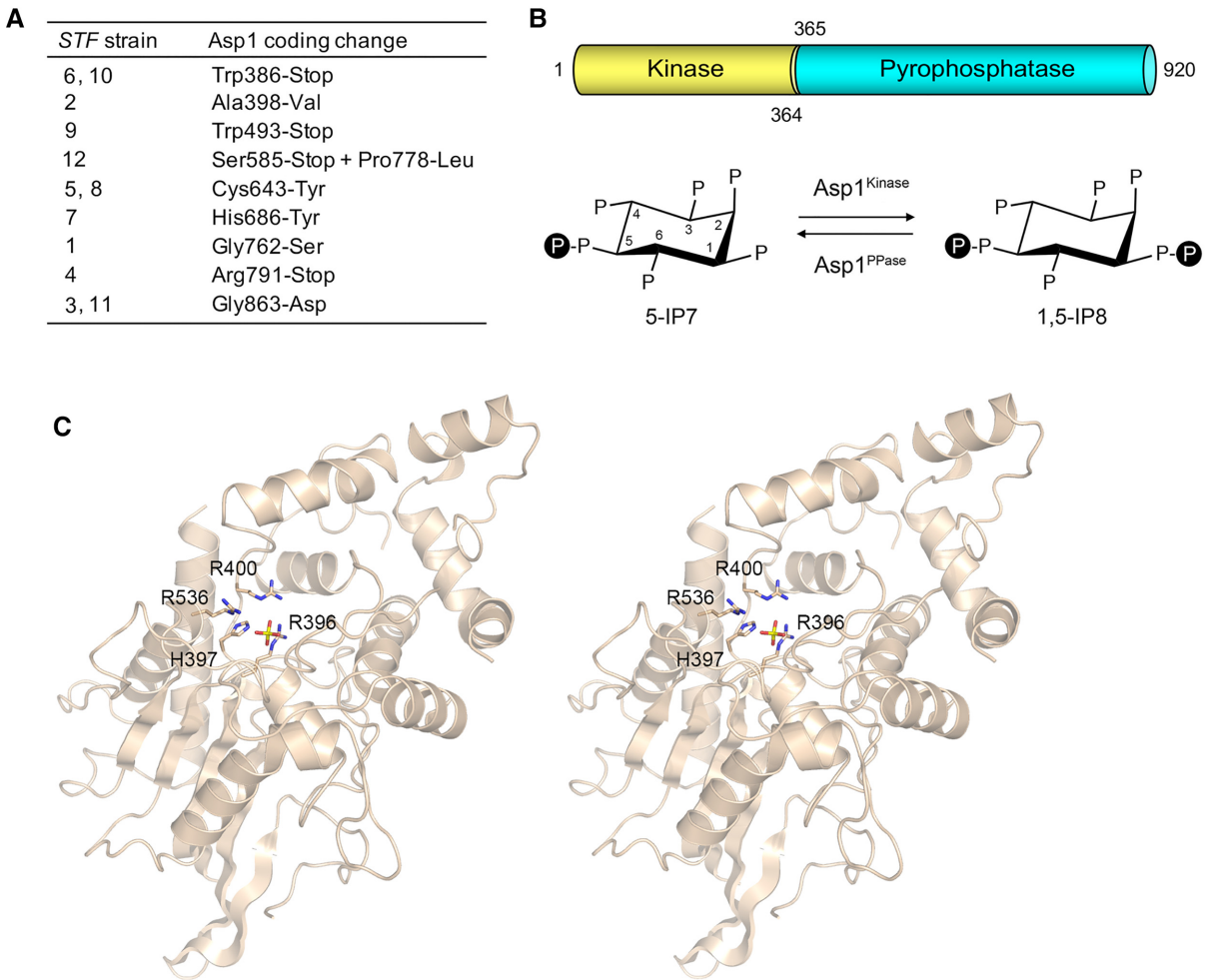

Figure 2. *STF* mutations map to the Asp1 IPP pyrophosphatase domain. (**A**) Whole-genome sequencing of 12 independent twice back-crossed *STF* strains revealed the indicated coding mutations in the C-terminal IPP pyrophosphatase domain of Asp1. (**B**) Asp1 is a bifunctional enzyme composed of an N-terminal IP7 kinase domain (gold) and a C-terminal IP8 pyrophosphatase domain (cyan). Asp1 kinase converts IP7 to IP8 and the Asp1 pyrophosphatase reverses this process, as shown. (**C**) Stereo view of the Phyre2 model of the Asp1 pyrophosphatase domain tertiary structure templated on the crystal structure of *Yersinia kristensenii* phytase, with a phosphate anion in the active site and surrounding active site side chains.

ing of two *CTD-T4A* pale progeny. Tetrads yielding three viable progeny ($n = 2$) were tetratypes (TT) comprising one *CTD-T4A* dark red haploid, one *CTD-T4A* pale haploid, and one *CTD-WT* light red haploid. Failure to recover the fourth *CTD-WT* dark red haploid indicated that the *asp1-(W493-Stop)* mutation, which eliminates the Asp1 pyrophosphatase domain while preserving the Asp1 kinase, is lethal in a wild-type *rpb1-CTD* background. We also dissected eight individual four-spore asci from the *STF-6* backcross. Tetrad analysis revealed three parental ditypes with four viable progeny, three non-parental ditypes with two viable progeny, and two tetratypes with three viable progeny. Thus, the *asp1-(W386-Stop)* allele is also lethal in the context of a wild-type Pol2 CTD.

Other *STF* alleles are viable but sick in a wild-type *rpb1-CTD* background

We then proceeded to mate the other *STF CTD-T4A* strains with a differentially marked wild-type *rpb1-CTD* strain and performed both random spore analysis and tetrad dissections as described above. *STF-1*, *STF-2*, *STF-4*, and *STF-12* matings to a wild-type *rpb1-CTD* strain yielded *CTD-WT STF* colonies at 30°C that stained deep red in the agar overlay assay. Red-staining *CTD-WT STF-3*, *STF-5*, and *STF-7* haploids were also viable but grew out more slowly than the other strains after sporulation. Sequencing the *asp1* pyrophosphatase domain ORF in these *CTD-WT* haploids affirmed the presence of the *STF* mutations. The *CTD-WT STF* strains were spot-tested for growth on YES agar medium. The *STF-1*, *STF-2*, *STF-3*, *STF-5*, *STF-7*, and *STF-12* mutations conferred a severe *cs* growth defect at 20 and 25°C, a *ts* growth defect at 34 and 37°C, and slower growth at 30°C compared to the *CTD-WT asp1*$^+$ control (Figure 4A). *CTD-WT STF-4* cells displayed a *cs* growth defect, but grew well at 30°C and better than the other *STF* strains at 25, 34 and 37°C (Figure 4A).

The viable *CTD-WT STF* strains were grown in phosphate-replete medium at 30°C and assayed for acid phosphatase activity. The *STF-1*, *STF-2*, *STF-3*, *STF-4*,

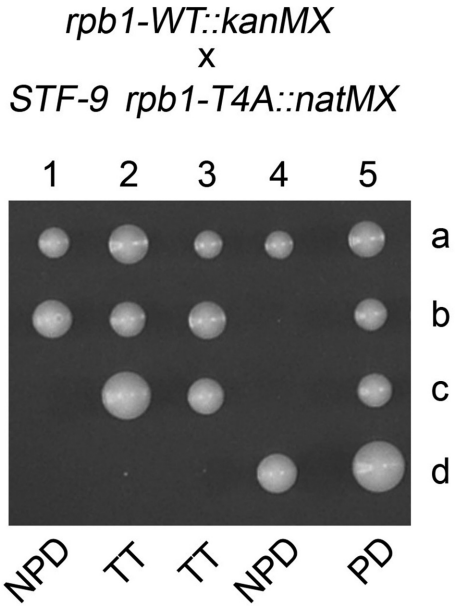

Figure 3. Tetrad dissection shows that *STF-9* is lethal in the context of a wild-type Pol2 CTD. Individual spores (a–d) from five tetrads (1-5) resulting from of a cross between *asp1-STF-9 CTD-T4A* and *asp1-WT CTD-WT* strains were arrayed on YES agar medium and incubated for 6 days at 30°C. Genotyping the viable progeny assigned the segregation patterns as non-parental ditype (NPD), parental ditype (PD), and tetratype (TT) as indicated.

STF-5, *STF-7,* and *STF-12* mutations increased Pho1 expression by 21-, 20-, 23-, 17-, 22-, 25-, and 21-fold, respectively, *vis-à-vis* the *CTD-WT asp1*$^{+}$ control (Figure 4B). Moreover, Pho1 expression in *STF-1*, *STF-2*, *STF-3*, *STF-4*, *STF-5*, *STF-7* and *STF-12* cells was 4-, 4-, 3-, 4-, 4-, 3-, and 3-fold higher in the *CTD-WT* background than in the *CTD-T4A* background (Figure 4B versus 1B). Thus, Asp1 pyrophosphatase and CTD Thr4 exert autonomous and opposing effects on Pho1 expression.

Lethality of *asp1-(W386-Stop)* and *asp1-(W493-Stop)* is suppressed by CPF and Rhn1 mutations

Fission yeast CPF is a 13-subunit protein assembly responsible for the co-transcriptional 3′ processing of Pol2 transcripts that precedes Pol2 transcription termination (41). Five of the CPF subunits (Ctf1, Ssu72, Dis2, Ppn1, and Swd22) are dispensable for growth. Rhn1 is an inessential CTD-binding Pol2 termination factor that recognizes the Thr4-PO_4 CTD mark (42). Loss-of-function mutants of Rhn1 or any of the five inessential CPF subunits result in hyper-repression of *pho1* RNA expression and Pho1 acid phosphatase activity in phosphate-replete cells (10). In light of the findings above that the *STF-6 asp1-(W386-Stop)* and *STF-9 asp1-(W493-Stop)* alleles were viable in combination with *CTD-T4A* (which is thought to exert a negative effect on 3′ processing/termination) but lethal in a wild-type *rpb1-CTD* background, we queried whether their lethality could be suppressed by non-CTD mutations in the 3′ processing/termination machinery. Accordingly, we performed pairwise matings of *STF-6 CTD-T4A* and *STF-9 CTD-T4A* strains with *dis2*Δ, *ctf1*Δ, *ssu72-C13S*, *ppn1*Δ, *swd22*Δ, and *rhn1*Δ strains. A population of random spores was screened for the drug-resistance markers linked to the *CTD-T4A* locus and the *CPF/rhn1* mutant loci. Haploid progeny bearing mutant *CPF/rhn1* alleles and were wild-type with respect to the Pol2 CTD were then screened by agar overlay for Pho1 expression, which showed similar numbers of pale and red isolates in every genetic cross. The viable *STF-6 CPF/rhn1* and *STF-9 CPF/rhn1* double-mutants were spot-tested for growth on YES agar in parallel with the respective *CPF/rhn1* single-mutants (Figure 5). Notable findings were that the *STF-6* and *STF-9* alleles alleviated the cold-sensitive growth defects of *ppn1*Δ and *swd22*Δ cells at 20°C and the slow-growth *ts* phenotype of *rhn1*Δ cells at 37°C. Also, the *rhn1*Δ *STF-6* and *rhn1*Δ *STF-9* double-mutants displayed a strong *cs* defect that was not seen in *rhn1*Δ *per se* (Figure 5). These genetic suppression data suggest that the lethality of the IPP pyrophosphatase-defective *asp1-(W386-Stop)* and *asp1-(W493-Stop)* mutations is exerted via 3′ processing/termination.

The *STF CPF/rhn1* double mutants were assayed for Pho1 acid phosphatase activity during growth in phosphate-replete medium, in parallel with the respective *CPF/rhn1* single mutants. In every case, the *STF* alleles elicited a strong de-repression of Pho1 expression, ranging in magnitude from 16- to 62-fold above the hyper-repressed level of Pho1 expression in the corresponding *CPF/rhn1* single mutants (Figure 6).

Transcriptome profiling of the *STF-6* and *STF-9* strains

We performed RNA-seq on poly(A)$^{+}$ RNA isolated from *STF-6* and *STF-9* cells and from the parental *rpb1-CTD-T4A* strain. cDNAs obtained from three biological replicates (using RNA from cells grown to mid-log phase in YES medium at 30°C) were sequenced for each strain. In the datasets, 90–96% of the reads were mapped to unique genomic loci (Supplementary Figure S1). Read densities (RPKM) for individual genes were highly reproducible between biological replicates (Pearson coefficients of 0.97–0.99; Supplementary Figure S2). A cutoff of ±2-fold change in normalized transcript read level and an adjusted *P*-value of ≤0.05 were the criteria applied to derive an initial list of differentially expressed annotated loci in the *STF-6* and *STF-9* mutants versus the parental *CTD-T4A* control. We then focused on differentially expressed genes with average normalized read counts ≥100 in either the *STF* or parental *T4A* strains in order to eliminate many (mostly non-coding) transcripts that were expressed at very low levels in vegetative cells. We thereby identified sets of 64 and 63 annotated protein-coding genes that were upregulated by these criteria in *STF-6* and *STF-9* cells, respectively, 51 of which were coordinately upregulated by ≥2-fold in both *STF* mutants ($P < 6.795e\text{-}98$) (Figure 7). The most highly upregulated sub-set (>16-fold increase) includes all three phosphate homeostasis genes: *pho1* (up 46- to 54-fold), *tgp1* (up 19- to 26-fold), and *pho84* (up 16- to 18-fold) (Figure 7). RNA-seq revealed no increase in *STF-6* and *STF-9* cells of the mRNA encoding Pho7, the transcription factor that drives *pho1*, *pho84*, and *tgp1* mRNA synthesis. The *ecl3*

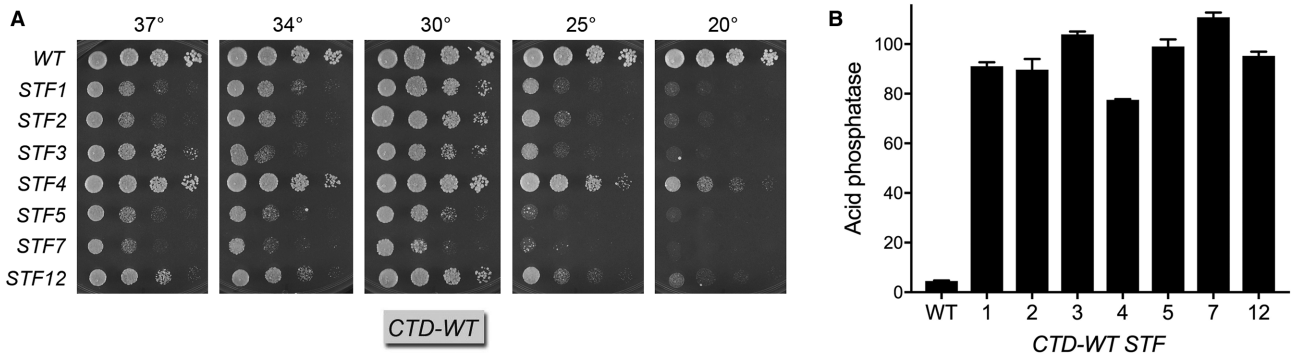

Figure 4. *STF* mutants that are viable with a wild-type *rpb1-CTD* elicit conditional growth defects and lead to stronger *pho1* de-repression than in the *CTD-T4A* background. (**A**) *CTD-WT* and *CTD-WT STF* strains (as specified on the left) were spot tested for growth at the indicated temperatures. (**B**) The *CTD-WT* and indicated *CTD-WT STF* strains were assayed for Pho1 acid phosphatase activity.

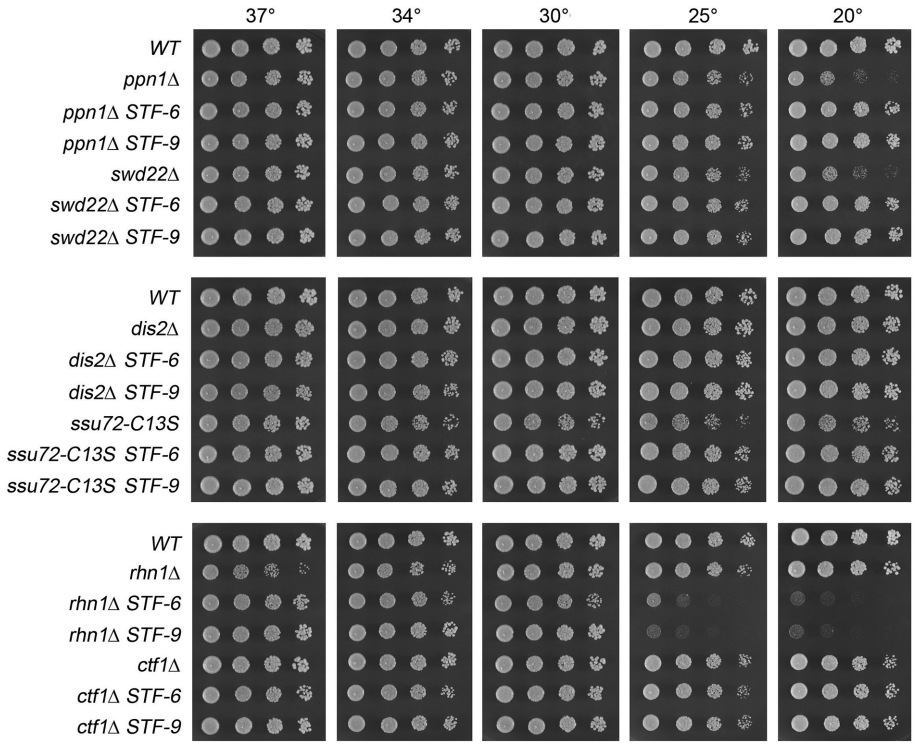

Figure 5. Lethality of *asp1-(W386-Stop)* and *asp1-(W493-Stop)* is suppressed by CPF and Rhn1 mutations. Serial 5-fold dilutions of the indicated strains were spot tested for growth at the indicated temperatures.

gene, upregulated by 28- to 39-fold, is located on chromosome II, adjacent to and in opposite orientation to the *prt2* lncRNA gene of the phosphate-regulated *prt2–pho84–prt–pho1* gene cluster (14). Two other genes involved in phosphate acquisition were also upregulated: SPBPB2B2.06c encoding an extracellular 5′ nucleotidase (up 28- to 48-fold) and SPBC1683.01 encoding a transmembrane phosphate transporter (up 3- to 4-fold) (Figure 7). It is suggested that *ecl3* and SPBC1683.01, in common with the three *PHO* genes, might be subject to transcription interference by 5′ flanking lncRNAs (29).

The RNA-seq experiment identified 63 and 65 protein-coding genes that were downregulated by ≥2-fold in *STF-6* and *STF-9* cells, respectively, 59 of which were coordinately downregulated in both *STF* mutants ($P < 2.152e\text{-}125$) (Supplementary Figure S4). The set of downregulated transcripts includes those encoding proteins involved in fission yeast iron homeostasis: the siderophore Str1; sulfiredoxin Srx1; ferric reductase Frp1, iron oxidase-permease Fio1; iron permease Fip1; and ferric reductase Frp2. Expression of these genes is normally repressed during growth in rich medium by the iron-sensing DNA-binding GATA-family transcriptional repressor Fep1 (43,44). RNA-seq showed no effect of *STF-6 or STF-9* on the level of *fep1*$^+$ mRNA compared to that in *T4A* cells, suggesting that the observed reduction in iron regulon transcripts is not caused by increased expression of the Fep1 repressor.

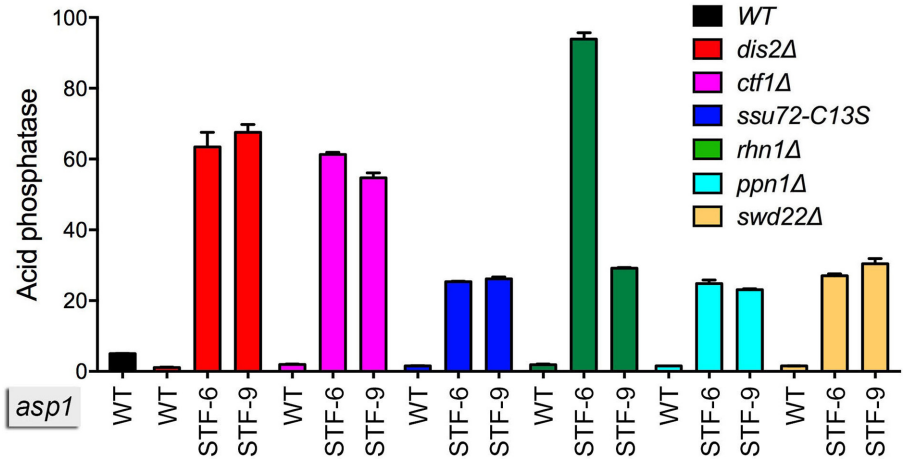

Figure 6. *STF-6* and *STF-9* alleles elicit strong de-repression of Pho1 in *STF CPF/rhn1* double mutants. Strains bearing the indicated *asp1* alleles (wild-type, *STF-6* or *STF-9*) in combination with CPF subunit or Rhn1 mutations as specified were grown in liquid culture at 30°C and assayed for acid phosphatase activity.

Identification of additional *STF* mutations by focused sequencing of the *asp1* locus

In light of the whole-genome sequencing data showing that all of the initial set of 12 *STF* strains had Asp1 pyrophosphatase mutations, we analyzed a second set of six independent twice-backcrossed *STF* isolates (alleles 13–18) by focused PCR amplification of the Asp1 pyrophosphatase ORF and sequencing the PCR product. We thereby found that all six had mutations in the Asp1 pyrophosphatase domain, including one nonsense change (Trp642-Stop) and four missense changes—Arg396His, Arg400His (two independent isolates), Glu844Lys, and Gly863Asp (Figure 8B). The Asp1 Gly863Asp lesion in the *STF-14* strain was identical to the missense mutations identified by whole genome sequencing in two independent *STF* mutants in the initial set (*STF-3*, *STF-11*). Moreover, the acid phosphatase activity of *STF-14* cells (Figure 8A) was similar to that of *STF-3* and *STF-11* cells (Figure 1B). The other *STF* strains in this set expressed lower levels of Pho1, albeit still 9- to 10-fold higher than the parental *T4A* strain (Figure 8A). Reference to the Phyre2 model (Figure 2C) underscores that the sites of two *STF* mutations—Arg396 and Arg400—are catalytic residues of the pyrophosphatase active site. It is conceivable that single Arg-to-His changes at these positions do not completely eliminate IPP pyrophosphatase activity, insofar as histidine might fulfill some of the interactions made by arginine with the scissile phosphate.

Second-round *STF* mutants that are viable with a wild-type *rpb1-CTD* elicit stronger *pho1* de-repression than in the *CTD-T4A* background

The *STF-13*, *STF-15*, *STF-16*, *STF-17,* and *STF-18* strains from the second set of *CTD-T4A STF* mutants were mated to a wild-type *rpb1-CTD* strain, the resulting diploids were sporulated, and random haploid progeny were screened for the *rpb1*-linked drug-resistance markers and for Pho1 expression by agar overlay. In each case, we recovered viable *CTD-WT* dark red isolates at the frequency expected for random segregation, signifying that the *asp1-E844K*, *asp1-W642Stop*, *asp1-R396H,* and *asp1-R400H* alleles were not lethal in the context of a wild-type Pol2 CTD. We infer that these mutations are likely hypomorphs with respect to Asp1 pyrophosphatase function. The *CTD-WT STF-13* and *STF-15* strains grew well on YES agar at all temperatures (Figure 8C). The *CTD-WT STF-16* and *STF-17* strains grew well at 30–37°C but displayed a slow growth defect at low temperatures, as gauged by colony size (Figure 8C). Testing the *CTD-WT STF* strains for acid phosphatase activity (Figure 8D) was instructive in the following respects: (i) the *STF-13*, *STF-15*, *STF-16,* and *STF-17* mutations increased Pho1 expression by 12-, 9-, 16-, and 16-fold, respectively, *vis-à-vis* the *asp1-WT* control; and (ii) Pho1 expression in cells bearing *STF-13*, *STF-15*, *STF-16*, and *STF-17* alleles was 8-, 6-, 11-, and 10-fold higher in the *CTD-WT* background than in the *CTD-T4A* background (Figure 8D versus A). These results fortify the conclusion that the Asp1 pyrophosphatase and the CTD Thr4 mark exert opposing effects on phosphate homeostasis.

DISCUSSION

The results of the *STF* screen and ensuing genetic analyses engender two key conclusions: (i) ablating the Asp1 IPP pyrophosphatase domain while leaving the IPP kinase domain intact can be lethal; and (ii) the IPP pyrophosphatase domain requirement for viability in such circumstances is bypassed by the *rpb1-CTD-T4A* mutation and by loss-of-function mutations in CPF subunits and termination factor Rhn1. The inference we draw is that an important role of the Asp1 pyrophosphatase is to constrain the level of IP8 or 1-IP7 synthesis catalyzed by the Asp1 kinase, without which IP8 or 1-IP7 may accumulate to toxic levels that elicit precocious termination by CPF/Rhn1.

We had already proposed that too much IP8 is toxic to fission yeast based on our findings that a viable IPP pyrophosphatase-defective allele—*asp1-H397A*, constructed by the Fleig laboratory (24)—was lethal in the absence of a second fission yeast IPP pyrophosphatase enzyme Aps1 (29). Aps1 is a member of the Nudix hydro-

gene	log2 change		protein / function
	STF-6	*STF-9*	
pho1	5.75	5.52	acid phosphatase
SPBPB2B2.06c	5.59	4.81	extracellular 5' nucleotidase
ecl3	5.29	4.83	extender of chronological lifespan
tgp1	4.69	4.28	glycerophosphodiester transporter
pho84	4.18	4.01	phosphate transporter
SPCC11E10.01	2.67	2.66	cystathionine beta-lyase
gpd3	2.55	2.12	glyceraldehyde 3-phosphate dehydrogenase
ngl1	2.34	2.43	peptide N-glycanase
SPBC1703.08c	2.31	2.34	5-formyltetrahydrofolate cyclo-ligase
isp4	2.18	2.08	oligopeptide transmembrane transporter
SPBC1683.01	2.01	1.77	phosphate transporter
gep4	1.91	2.05	phosphatidylglycerol phosphate phosphatase
aes1	1.84	1.82	phenazine biosynthesis
SPBC25B2.08	1.78	1.67	
rds1	1.72	1.48	ferritin related conserved fungal protein
SPAPB8E5.10	1.70	1.95	
SPBC8E4.04	1.57	1.49	alditol $NADP^+$ 1-oxidoreductase
sdu1	1.49	1.28	deubiquitinase/desumoylase
SPAC2H10.01	1.49	1.21	Zn2-Cys6 transcription factor
qcr8	1.46	1.52	ubiquinol-cytochrome-c reductase complex
oga1	1.45	1.26	Stm1 homolog
SPAC1039.01	1.44	1.25	amino acid transmembrane transporter
SPCC1235.01	1.42	1.50	
mcb1	1.41	1.21	MCM binding protein
mae1	1.37	1.30	malate/succinate:proton symporter
tpr1	1.37	1.47	Paf1 complex subunit
SPBPB7E8.01	1.37	1.33	GPI anchor protein
cyt1	1.32	1.18	cytochrome c1
tef101	1.30	1.25	translation elongation factor EF-1 alpha
mic26	1.29	1.12	MICOS complex subunit
pcm1	1.29	1.52	RNA cap guanine-N7 methyltransferase
tef102	1.28	1.21	translation elongation factor EF-1 alpha
wdr83	1.27	1.59	WD repeat protein
qcr6	1.26	1.44	ubiquinol-cytochrome-c reductase complex
SPBC3B8.08	1.23	1.28	
mae2	1.21	1.03	malate dehydrogenase
SPBC1703.13c	1.20	1.12	mitochondrial phosphate transporter
abp2	1.19	1.31	
slx4	1.18	1.31	structure-specific endonuclease
mug2	1.13	1.04	DUF1773 family protein
set10	1.13	1.07	lysine methyltransferase
mef1	1.11	1.26	mitochondrial translation elongation factor G
SPBC26H8.11c	1.10	1.06	acyl-coenzyme A thioesterase
SPBPB21E7.09	1.09	1.07	L-asparaginase
aah2	1.09	1.03	alpha-amylase
leo1	1.09	1.19	Paf1 complex subunit
mic19	1.08	1.05	MICOS complex subunit
cox13	1.07	1.18	cytochrome c oxidase subunit
cnp3	1.06	1.25	kinetochore protein CENP-C
mfs3	1.06	1.13	spermidine transporter
cox12	1.01	1.00	cytochrome c oxidase subunit

Figure 7. Transcription profiling identifies genes upregulated by *STF-6* and *STF-9* alleles. List of 51 annotated protein-coding genes that were upregulated at least 2-fold in *STF-6 T4A* and *STF-9 T4A* cells compared the parental *T4A* strain. The log2 fold changes are shown. The 13 genes that were also upregulated in *asp1-H397A* cells are indicated in bold font.

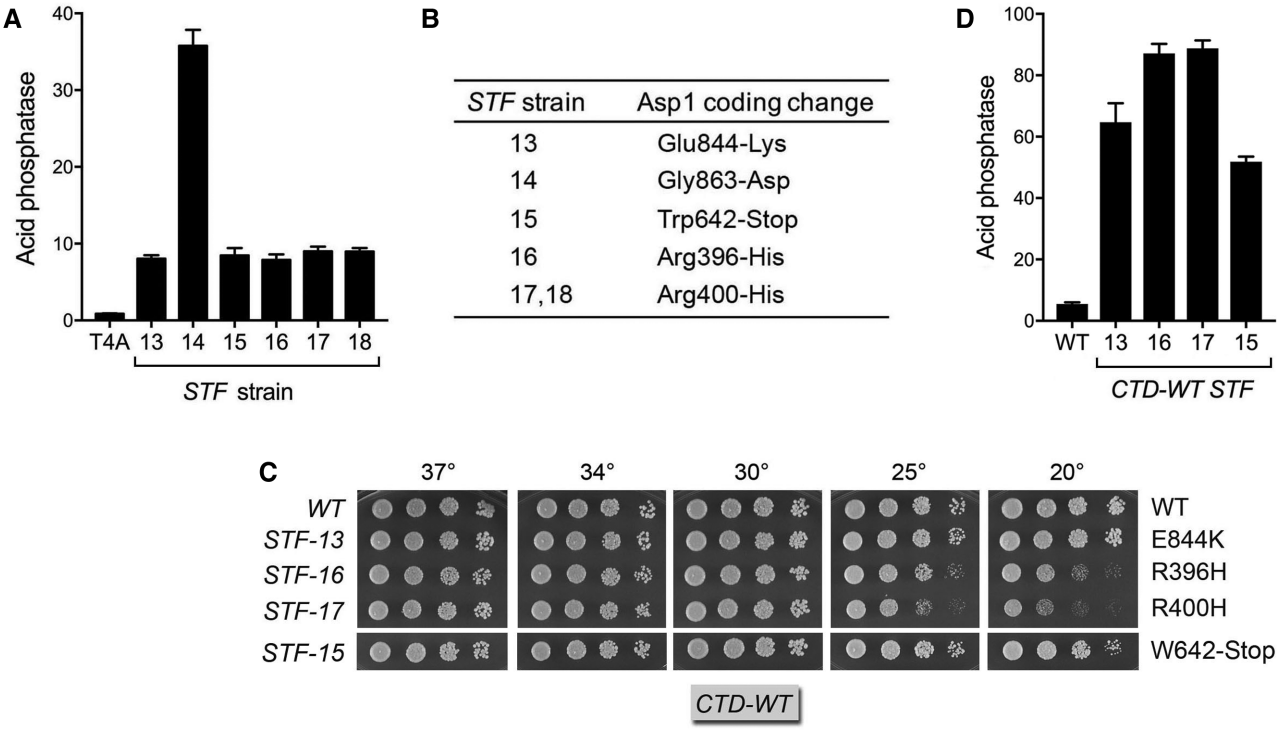

Figure 8. 'Second round' *STF* mutants are viable with a wild-type *rpb1-CTD* and elicit stronger *pho1* de-repression than in the *CTD-T4A* background. (**A**) The parental *T4A* and derived *STF* strains were assayed for Pho1 acid phosphatase activity. (**B**) Sequencing of PCR-amplified *asp1* loci from six independent twice back-crossed *STF* strains revealed the coding mutations in the C-terminal pyrophosphatase domain of Asp1, as specified. (**C**) The *CTD-WT* and *CTD-WT STF* strains (as specified on the left) were spot tested for growth at the indicated temperatures. The Asp1 coding changes are indicated at right. (**D**) The *CTD-WT* and *CTD-WT STF* strains were assayed for Pho1 acid phosphatase activity.

lase superfamily (45). Moreover, the synthetic lethality of *asp1-H397A aps1*Δ was suppressed by *rpb1-CTD-T4A* and by mutations of CPF subunits Ppn1, Swd22, Ssu72, and Ctf1 (29). These and other data, especially the effects of altered IP8 (or 1-IP7) levels on *PHO* gene expression, collectively pointed to IP8 (or 1-IP7) as an agonist of 3′ processing/termination. Accordingly, absence of IP8/1-IP7 in *asp1*Δ cells (26) resulted in *PHO* gene hyper-repression (29); increased IP8 in *asp1-H397A* cells (26) resulted in de-repression of the *PHO* regulon under phosphate-replete conditions (29); and too much 1-IPPs in *asp1-H397A aps1*Δ cells elicited lethal precocious termination events affecting one or more essential fission yeast genes. Two key observations *vis-à-vis* the *STF* phenomenon are: (i) whereas the *CTD-T4A* mutation erased the strong de-repression of Pho1 by *asp1-H397A*, the low level of Pho1 expression in the phosphate-replete *CTD-T4A asp1-H397A* double-mutant was nonetheless 5-fold higher than that in hyper-repressed *CTD-T4A* single-mutant cells (29), i.e. in retrospect, *asp1-H397A* had a weak but detectable *STF* phenotype; and (ii) Pho1 de-repression 'won out' over *T4A* repression in the viable *asp1-H397A aps1*Δ *CTD-T4A* strain (29). These findings suggest that there is a threshold level of IP8 (or 1-IP7), above which precocious lncRNA termination is insensitive to loss of the CTD Thr4 mark.

A conundrum here is why the *asp1-*(*W386-Stop*) and *asp1-*(*W493-Stop*) nonsense alleles that emerged from the *STF* screen, which truncate all or most of the Asp1 pyrophosphatase domain, do not phenocopy the *asp1-H397A* allele used in prior studies (29), i.e. *asp1-*(*W386-Stop*) and *asp1-*(*W493-Stop*) fail to grow in a *CTD-WT* background whereas *asp1-H397A CTD-WT* cells grow well at all temperatures tested. Rather, *asp1-*(*W386-Stop*) and *asp1-*(*W493-Stop*) mimic the lethality and *PHO* de-repressive phenotypes observed for the *asp1-H397A aps1*Δ double pyrophosphatase-dead strain. A possible distinction is that the *asp1-STF* mutations are in the context of an otherwise unperturbed chromosomal *asp1* locus, whereas the *asp1-H397A* strain was constructed by replacing the *asp1*$^+$ gene with a marked mutant allele that is flanked by a kanamycin-resistance gene cassette (24). The *asp1-H397A–kanMX* junction in the *asp1-H397A* strain is such that the promoter element for the *kanMX* cassette was inserted 6 nt downstream of the *asp1*$^+$ ORF stop codon, signifying that the native *asp1*$^+$ poly(A) site and terminator were displaced during mutant construction. This raised the possibility that the level of *asp1-H397A* expression in the *asp1-H397A–kanMX* strain, and hence the level of unopposed Asp1 IPP kinase activity, might differ from that of an *asp1-STF* strain in which there is no 3′ flanking marker. To address this point, we introduced a *kanMX* cassette 6 nt downstream of the 'native' *asp1*$^+$ stop codon in the *STF-6*, *STF-9*, *STF-2* and *STF-12* mutant strains. The marked *STF* strains were mated to a wild-type *rpb1-CTD* strain and a large population of random haploid progeny was screened for the drug-resistance markers linked to the *asp1-STF* and *rpb1-CTD-WT* genes. Failure to recover any doubly drug-resistant *STF-6* or *STF-9* haploids signified that the lethal-

ity of the *asp1-STF-6* and *asp1-STF-9* alleles in a wild-type background could not be suppressed by the presence of a 3′ flanking gene analogous to that of the Fleig lab's *asp1-H397A* strain. Doubly marked *STF-2 CTD-WT* and *STF-12 CTD-WT* haploids were recovered and they displayed growth defects comparable to those seen in Figure 4A for the *STF-2 CTD-WT* and *STF-12 CTD-WT* strain in which the *asp1-STF* alleles were unmarked.

An alternative conjecture is that binding of IP8 (or 1-IP7) to the active site of the C-terminal pyrophosphatase domain of Asp1 exerts a negative effect (presumably allosteric) on the activity of the N-terminal IPP kinase domain. This scenario resonates with hypotheses of inter-domain allosteric communication for bifunctional mammalian IPP kinase/pyrophosphatase enzymes put forward by the Shears laboratory (46). Based on structures of histidine acid phosphatase enzymes, we envision that simple replacement of the histidine nucleophile by alanine, which obviously impairs catalysis, ought not to interdict the binding of the substrate to the Asp1 pyrophosphatase active site and hence not preclude the hypothetical allosteric effect on the kinase. By contrast, elimination of the pyrophosphatase domain (by a premature stop codon at or near the proximal margin of the pyrophosphatase domain) would certainly eliminate IP8 (or 1-IP7) binding and hence the potential for exerting a brake allosterically on the IPP kinase. A similar dampening of an allosteric effect might ensue from a missense mutation that locally distorts the pyrophosphatase active site and thereby compromises IP8 binding.

We posit that there is a narrow threshold around which the level of unopposed (or weakly opposed) Asp1 kinase activity becomes toxic or growth inhibitory, in which case *STF* mutations in the Asp1 pyrophosphatase domain might perturb the steady state levels or intracellular distribution of the Asp1 protein (even modestly), and thus the level of Asp1 IPP kinase activity, thereby leading to variable mutational effects on vegetative growth. There is an apparent trend whereby the *STF* pyrophosphatase mutations that most strongly suppress *CTD-T4A* with respect to Pho1 activity (Figure 1B) have more severe effects on vegetative growth in the *CTD-WT* background (Figures 3 and 4A) than do 'second-round' *STF* mutations that are relatively weaker *T4A* suppressors (Figure 8A and C).

The present transcriptome analysis of the *STF-6* and *STF-9 asp1* pyrophosphatase truncation mutants reveals a set of 51 coding genes that are coordinately upregulated compared to the parental *CTD-T4A* strain. We had previously identified 63 coding genes over-expressed in *asp1-H397A* cells versus wild-type *asp1*$^{+}$ (29). Of these, 32/63 are upregulated in *STF-6* cells and 16/63 are up-regulated in *STF-9* cells. Most pertinent is that 13 of the genes that were overexpressed in *asp1-H397A* were coordinately over-expressed in both *STF-6* and *STF-9*. These 13 are indicated in bold font in Figure 7 and include all three genes of the *PHO* regulon that are normally repressed by upstream flanking lncRNAs and are hyper-repressed by *CTD-T4A*. With respect to the 59 protein-coding genes that were down-regulated in *STF-6* and *STF-9* cells compared to the parental *T4A* strain, 11 of them were also downregulated in *asp1-H397A* cells (indicated in bold font in Supplementary Figure S4), including four of the iron homeostasis genes. We conclude that there is a coherent ensemble of 1-IPP-responsive genes dysregulated by inactivation of the Asp1 pyrophosphatase, be it by domain deletion or crippling of the active site and irrespective of CTD Thr4 status.

Finally, the successful implementation here of the *STF* screen rejuvenates and extends the power of classic forward genetics to illuminate the biology of the Pol2 CTD, which was initially practiced to great effect by the Young and Corden labs in the 1990s via their isolation of extragenic suppressors of budding yeast CTD truncations or S2A phospho-site mutations (47–50). The *SRB* (Suppressor of RNA polymerase B) screen was key to the identification via genetics of the subunits of the Pol2 holoenzyme (including components of the Mediator) that are essential for enhancer-dependent Pol2 transcription initiation. The present *STF* screen fortifies the connections between CTD Thr4 and IPP dynamics as governors of Pol2 termination in fission yeast.

DATA DEPOSITION

The RNA-seq data in this publication have been deposited in NCBI's Gene Expression Omnibus and are accessible through GEO Series accession number GSE155609. (https://www.ncbi.nlm.nih.gov/geo/query/acc.cgi?acc=GSE155609).

SUPPLEMENTARY DATA

Supplementary Data are available at NAR Online.

ACKNOWLEDGEMENTS

We thank Prof. Ursula Fleig for comments on the manuscript. The MSKCC Integrated Genomics Operation Core is supported by Cycle for Survival and the Marie-Josée and Henry R. Kravis Center for Molecular Oncology.

FUNDING

NIH [R01-GM52470, R01-GM134021, R35-GM126945]; NCI [P30 CA08748]. Funding for open access charge: NIH [R35-GM126945].
Conflict of interest statement. None declared.

REFERENCES

1. Eick,D. and Geyer,M. (2013) The RNA polymerase II carboxy-terminal domain (CTD) code. *Chem. Rev.*, **113**, 8456–8490.
2. Corden,J.L. (2013) RNA polymerase II C-terminal domain: tethering transcription to transcript and template. *Chem. Rev.*, **113**, 8423–8455.
3. Jeronimo,C., Bataille,A.R. and Robert,F. (2013) The writers, readers, and functions of the RNA polymerase II C-terminal domain code. *Chem. Rev.*, **113**, 8491–8522.
4. Harlen,K.M. and Churchman,L.S. (2018) The code and beyond: transcription regulation by the RNA polymerase II carboxy-terminal domain. *Nat. Rev. Mol. Cell Biol.*, **18**, 263–273.
5. Yurko,N.M. and Manley,J.L. (2018) The RNA polymerase II CTD "orphan" residues: emerging insights into the functions of Tyr-1, Thr-4, and Ser-7. *Transcription*, **9**, 30–40.
6. Schwer,B. and Shuman,S. (2011) Deciphering the RNA polymerase II CTD code in fission yeast. *Mol. Cell*, **43**, 311–318.
7. Schwer,B., Sanchez,A.M. and Shuman,S. (2012) Punctuation and syntax of the RNA polymerase II CTD code in fission yeast. *Proc. Natl. Acad. Sci. U.S.A.*, **109**, 18024–18029.

8. Schwer,B., Bitton,D.A., Sanchez,A.M., Bähler,J. and Shuman,S. (2014) Individual letters of the RNA polymerase II CTD code govern distinct gene expression programs in fission yeast. *Proc. Natl. Acad. Sci. U.S.A.*, **111**, 4185–4190.
9. Schwer,B., Sanchez,A.M. and Shuman,S. (2015) RNA polymerase II CTD phospho-sites Ser5 and Ser7 govern phosphate homeostasis in fission yeast. *RNA*, **21**, 1770–1780.
10. Sanchez,A.M., Shuman,S. and Schwer,B. (2018) RNA polymerase II CTD interactome with 3′ processing and termination factors in fission yeast and its impact on phosphate homeostasis. *Proc. Natl. Acad. Sci. U.S.A.*, **115**, E10652–E10661.
11. Chatterjee,D., Sanchez,A.M., Goldgur,Y., Shuman,S. and Schwer,B. (2016) Transcription of lncRNA *prt*, clustered *prt* RNA sites for Mmi1 binding, and RNA polymerase II CTD phospho-sites govern the repression of *pho1* gene expression under phosphate-replete conditions in fission yeast. *RNA*, **22**, 1011–1025.
12. Sanchez,A.M., Shuman,S. and Schwer,B. (2018) Poly(A) site choice and Pol2 CTD Serine-5 status govern lncRNA control of phosphate-responsive *tgp1* gene expression in fission yeast. *RNA*, **24**, 237–250.
13. Carter-O'Connell,I., Peel,M.T., Wykoff,D.D. and O'Shea,E.K. (2012) Genome-wide characterization of the phosphate starvation response in *Schizosaccharomyces pombe*. *BMC Genomics*, **13**, 697.
14. Garg,A., Sanchez,A.M., Shuman,S. and Schwer,B. (2018) A long noncoding (lnc) RNA governs expression of the phosphate transporter Pho84 in fission yeast and has cascading effects on the flanking *prt* lncRNA and *pho1* genes. *J. Biol. Chem.*, **293**, 4456–4467.
15. Shah,S., Wittmann,S., Kilchert,C. and Vasiljeva,L. (2014) lncRNA recruits RNAi and the exosome to dynamically regulate *pho1* expression in response to phosphate levels in fission yeast. *Genes Dev.*, **28**, 231–244.
16. Lee,N.N., Chalamcharia,V.R., Reyes-Turce,F., Mehta,S., Zofall,M., Balachandran,V., Dhakshnamoorthy,J., Taneja,N., Yamanaka,S., Zhou,M. *et al.* (2013) Mtr4-like protein coordinates nuclear RNA processing for heterochromatin assembly and for telomere maintenance. *Cell*, **155**, 1061–1074.
17. Ard,R., Tong,P. and Allshire,R.C. (2014) Long non-coding RNA-mediate transcriptional interference of a permease gene confers drug tolerance in fission yeast. *Nat. Commun.*, **5**, 5576.
18. Schwer,B., Sanchez,A.M., Garg,A., Chatterjee,D. and Shuman,S. (2017) Defining the DNA binding site recognized by the fission yeast Zn_2Cys_6 transcription factor Pho7 and its role in phosphate homeostasis. *mBio*, **8**, e01218-17.
19. Garg,A., Goldgur,Y., Schwer,B. and Shuman,S. (2018) Distinctive structural basis for DNA recognition by the fission yeast Zn_2Cys_6 transcription factor Pho7 and its role in phosphate homeostasis. *Nucleic Acids Res.*, **46**, 11262–11273.
20. Garg,A., Goldgur,Y., Sanchez,A.M., Schwer,B. and Shuman,S. (2019) Structure of fission yeast transcription factor Pho7 bound to *pho1* promoter DNA and effect of Pho7 mutations on DNA binding and phosphate homeostasis. *Mol. Cell. Biol.*, **39**, e00132-19.
21. Gross,T. and Käufer,N.F. (1998) Cytoplasmic ribosomal protein genes of the fission yeast *Schizosaccharomyces pombe* display a unique promoter type: a suggestion for nomenclature of cytoplasmic ribosomal proteins in databases. *Nucleic Acids Res.*, **26**, 33019–33322.
22. Witt,I., Straub,N., Käufer,N.F. and Gross,T. (1993) The CAGTCACA box in the fission yeast *Schizosaccharomyces pombe* functions like a TATA element and binds a novel factor. *EMBO J.*, **12**, 1201–1203.
23. Witt,I., Kwart,M., Groβ,T. and Käufer,N.F. (1995) The tandem repeat AGGGTAGGGT is, in the fission yeast, a proximal activation sequence and activates basal transcription mediated by the sequence TGTGACTG. *Nucleic Acids Res.*, **23**, 4296–4302.
24. Pöhlmann,J. and Fleig,U. (2010) Asp1, a conserved 1/3 inositol polyphosphate kinase, regulates the dimorphic switch in *Schizosaccharomyces pombe*. *Mol. Cell. Biol.*, **30**, 4535–4537.
25. Topolski,B., Jakopec,J., Künzel,N.A. and Fleig,U. (2016) Inositol pyrophosphate kinase Asp1 modulates chromosome segregation fidelity and spindle function in *Schizosaccharomyces pombe*. *Mol. Cell. Biol.*, **36**, 3128–3140.
26. Pascual-Ortiz,M., Saiardi,A., Walla,E., Jakopec,V., Künzel,N.A., Span,I., Vangala,A. and Fleig,U. (2018) Asp1 bifunctional activity modulates spindle function via controlling cellular inositol pyrophosphate levels in *Schizosaccharomyces pombe*. *Mol. Cell. Biol.*, **38**, e00047-18.
27. Randall,T.A., Gu,C., Wang,H. and Shears,S.B. (2020) A two-way switch for inositol pyrophosphate signaling: evolutionary history and biological significance of a unique, bifunctional kinase/phosphatase. *Adv. Biol. Regul.*, **75**, 100674.
28. Dollins,D.E., Bai,W., Fridy,P.C., Otto,J.C., Neubauer,J.L., Gattis,S.G., Mehta,K.P. and York,J.D. (2020) Vip1 is a kinase and pyrophosphatase switch that regulates inositol diphosphate signaling. *Proc. Natl. Acad. Sci. U.S.A.*, **117**, 9356–9364.
29. Sanchez,A.M., Garg,A., Shuman,S. and Schwer,B. (2019) Inositol pyrophosphates impact phosphate homeostasis via modulation of RNA 3′ processing and transcription termination. *Nucleic Acids Res.*, **47**, 8452–8469.
30. Moreno,S., Klar,A. and Nurse,P. (1991) Molecular genetic analysis of fission yeast *Schizosaccharomyces pombe*. *Methods Enzymol.*, **194**, 795–823.
31. Langmead,B. and Salzberg,S. (2012) Fast gapped-read alignment with Bowtie 2. *Nat. Methods*, **9**, 357–359.
32. Li,H., Handsaker,B., Wysoker,A., Fennell,T., Ruan,J., Homer,N., Marth,G., Abecasis,G. and Durbin,R. (2009) The sequence alignment/map format and SAMtools. *Bioinformatics*, **25**, 2078–2079.
33. Li,H. (2011) A statistical framework for SNP calling, mutation discovery, association mapping and population genetical parameter estimation from sequencing data. *Bioinformatics*, **27**, 2987–2993.
34. Cingolani,P., Platts,A., Wang,L., Coon,M., Nguyen,T., Wang,L., Land,S.J., Lu,X. and Ruden,D.M. (2012) A program for annotating and predicting the effects of single nucleotide polymorphisms, SnpEff: SNPs in the genome of *Drosophila melanogaster* strain w1118; iso-2; iso-3. *Fly*, **6**, 80–92.
35. Kim,D., Langmead,B. and Salzberg,S.L. (2015) HISAT: a fast spliced aligner with low memory requirements. *Nat. Methods*, **12**, 357–360.
36. Pyl,P.T, Anders,S. and Huber,W. (2014) HTSeq—a Python framework to work with high-throughput sequencing data. *Bioinformatics*, **31**, 166–169
37. Love,M.I., Huber,W. and Anders,S. (2014) Moderated estimation of fold change and dispersion for RNA-seq data with DESeq2. *Genome Biol.*, **15**, 550.
38. Schweingruber,M.E., Schweingruber,A.M. and Schüpbach,M.E. (1982) Isolation and characterization of acid phosphatase mutants in *Schizosaccharomyces pombe*. *Curr. Genet.*, **5**, 109–117.
39. Ariza,A., Moroz,O.V., Blagova,E.V., Turkenburg,J.P., Waterman,J., Roberts,S.M., Vind,J., Sjøholm,C., Lassen,S.F., De Maria,L. *et al.* (2013) Degradation of phytate by the 6-phytase from *Hafnia alvei*: a combined structural and solution study. *PLoS One*, **8**, e65062.
40. Kelley,L.A., Mezulis,S., Yates,C.M., Wass,M.N. and Sternberg,J.E. (2015) The Phyre2 web portal for protein modeling, prediction and analysis. *Nat. Protoc.*, **10**, 845–858.
41. Vanoosthuyse,V., Legros,P., van der Sar,S.J., Yvert,G., Toda,K., Le Bihan,T., Watanabe,Y., Hardwick,K. and Bernard,P. (2014) CPF-associated phosphatase activity opposes condensin-mediated chromosome condensation. *PLos Genet.*, **10**, e1004415.
42. Jasnovidova,O., Krejcikova,M., Kubicek,K. and Stefl,R. (2017) Structural insight into recognition of phosphorylated threonine-4 of RNA polymerase II C-terminal domain by Rtt103p. *EMBO Rep.*, **18**, 906–913.
43. Labbé,S., Pelletier,B. and Mercier,A. (2007) Iron homeostasis in the fission yeast *Schizosaccharomyces pombe*. *Biometals*, **20**, 523–537.
44. Rustici,G., van Bakel,H., Lackner,D.H., Holstege,F.C., Wijmenga,C., Bähler,J. and Brazma,A. (2007) Global transcriptional responses of fission and budding yeast to changes in copper and iron levels: a comparative study. *Genome Biol.*, **8**, R73.
45. Safrany,S.T., Ingram,S.W., Cartwright,J.L., Falck,J.R., McLennan,A.G., Barnes,L.D. and Shears,S.B. (1999) The diadenosine hexaphosphate hydrolase from *Schizosaccharomyces pombe* and *Saccharomyces cerevisiae* are homologues of the human disphoshoinositol polyphosphate phosphohydrolase: overlapping substrate specificities in a MutT-type protein. *J. Biol. Chem.*, **274**, 21735–21740.
46. Randall,T.A., Gu,C., Li,X., Wang,H. and Shears,S.B. (2020) A two-way switch for inositol pyrophosphate signaling: evolutionary history and biological significance of a unique, bifunctional kinase/phosphatase. *Adv. Biol. Regul.*, **75**, 100674.

47. Koleske,A.J., Buratowski,S., Nonet,M. and Young,R.A. (1992) A novel transcription factor reveals a functional link between the RNA polymerase II CTD and TFIID. *Cell*, **69**, 883–894.
48. Thompson,C.M., Koleske,A.J., Chao,D.M. and Young,R.A. (1993) A multisubunit complex associated with the RNA polymerase II CTD and TATA-binding protein in yeast. *Cell*, **73**, 1361–1375.
49. Yuryev,A. and Corden,J.L. (1996) Suppression analysis reveals a functional difference between the serines in positions two and five in the consensus sequence of the C-terminal domain of yeast RNA polymerase II. *Genetics*, **143**, 661–671.
50. Liao,S.M., Zhang,J., Jeffery,D.A., Koleske,A.J., Thompson,C.M., Chao,D.M., Viljoen,M., van Vuuren,H.J. and Young,R.A. (1995) A kinase-cyclin pair in the RNA polymerase II holoenzyme. *Nature*, **374**, 193–196.